Dynamic Characteristic Analysis and Force Loop Design for the Aerodynamic Load Simulator

Yoonsu Nam*

Department of Mechanical Engineering, Kangwon National University

A dynamic load simulator which can reproduce, on-ground, the aerodynamic hinge moment of control surface, is an essential rig for performance and stability test of aircraft actuation system. The hinge moment varies widely in the flight envelope depending on specific flight condition and maneuvering status. To replicate the wide spectrum of this hinge moment variation within some accuracy bounds, a force controller is designed based on the Quantitative Feedback Theory (QFT). A dynamic model of load actuation system is derived, and compared with the experimental results. Through this comparison, a nominal plant model of load actuation system with some uncertainty bounds is developed. The efficacy of QFT force controller is verified by numerical simulation, in which hydraulic actuation system dynamics of aircraft control surface is considered.

Key Words : QFT, Aerodynamic Load, Servo Valve

1. Introduction

Hydraulic actuation system is the common choice for driving aircraft control surface because of its high power to weight ratio, and stiffness to the external load. To prove the stability and performance of aircraft actuation system in the first-flight and future airborne operation, a lot of test procedures should be prepared, and successfully passed on-ground (Boeing Commercial Airplane Company, 1985). One of these is the loaded performance test, in which the aerodynamic loads on control surface are considered. The aerodynamic load, i. e. hinge moment, depends on the aircraft attitude (deflection of control surface, angle of attack, and etc.), and flight condition (Mach #, and height), and therefore varies wide in the whole flight envelope (Roskam, 1979). A special equipment called Dynamic Load Simulator (DLS), which can reproduce, on-ground, the aerodynamic hinge moment is required for this loaded test. Two independent actuation systems are needed for DLS. One is the real actuation system driving aircraft control surface, and the other is for aerodynamic load simulation. By setting up load actuator as counter acting with the control surface driving actuator, and designing an appropriate force control system for load actuator, DLS can be mechanized. By analyzing hinge moment variations due to deflection angle change of control surface in the whole flight envelope, a design specification for the load replication system can be drawn for any specific application (Nam, 2000). Obtaining an accurate mathematical model for the DLS is the first step to successfully design an aerodynamic load replication system. However, the dynamic characteristics of load actuation system using hydraulic power are basically nonlinear. This non-linearity mainly comes from the fluid flow dynamics through servo valve port (Merritt, 1967). Therefore, any LTI (Linear Time Invariant) model for DLS can not describe the whole system dynamics.

The purpose of this paper is to design a robust

* **E-mail** : nys@cc.kangwon.ac.kr
TEL : +82-33-250-6376 ; **FAX** : +82-33-257-4190
Department of Mechanical Engineering, Kangwon National University, 192-1, Hyoja 2-dong, Chunchon city, Kangwon-do 200-701, Korea. (Manuscript **Recevied** July 25, 2000; **Revised** September 20, 2000)

force control system for aerodynamic load simulator. Therefore, the contents of this paper are composed of two parts, i. e. derivation of a nominal plant model with the uncertainty bounds for DLS dynamics and a force control loop design using QFT. Two theoretical models are presented and tested for their validity with the experimental results in Sec. 2. The nonlinear dynamics of load actuation system is represented as a set of linear systems having parametric uncertainty model. A nominal model for DLS dynamics, and suitable uncertainty bounds are proposed by the comparison of this analytic model with the experimental results. Section 3 and 4 contain QFT force controller design procedures and some simulation results to verify the performance of QFT force loop design.

2. Mathematical Model of Dynamic Load Simulator

A schematic diagram of Dynamic Load Simulator (DLS) with the structure of pitch axis flight control system is shown in Fig. 1. DLS described in the upper part of Fig. 1 is composed of backup stiffness to simulate attachment effect of control surface driving actuator on airframe structure, a flywheel to imitate moment of inertia of control surface, and two actuation systems which represent control surface driving actuator and load replicating actuator. The force command for load actuation system comes from Flight Dynamics real time Simulation Computer (FMSC), which numerically solves the aircraft flight dynamics and the hinge moment for the given flight condition. Two different mathematical models (Model #1 & 2) for DLS are introduced and compared with the experimental results in this section. Whereas the complete linearized dynamics of control surface driving DDV actuator are considered in the model #1, only the simplified mechanical properties of DDV actuator are assumed in the model #2.

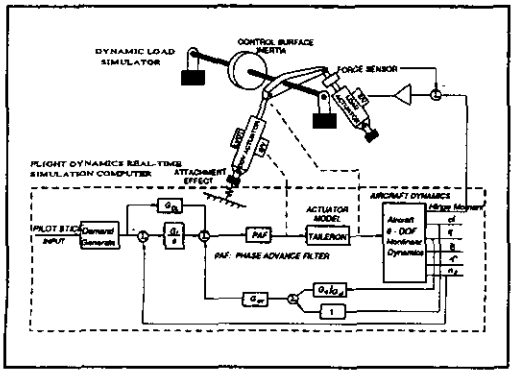

Fig. 1 Schematics of dynamic load simulator

2.1 Model #1 for DLS dynamics

Because of the apparent advantages in weight, size, and simplified fault monitoring mechanism compared to Electro Hydraulic Valve (EHV) actuation, the use of Direct Drive Valve (DDV) as a control surface driving actuator becomes a current trend in a modern flight control system design (Schaefer, Vieten 1993). The model of DDV actuator has complicated internal structure for performance enhancement and fault monitoring. However, the following simplified linear model is enough for this study.

DDV spool dynamics is determined by the following equations. In Eq. (1), the hydraulic Bernoulli flow forces, F_B are considered, because it is not negligible amount as opposed to the case of flapper nozzle type servo valve.

$$K_m i = M_v \frac{d^2 x_v}{dt^2} + B_v \frac{dx_v}{dt} + K_v x_v + \sum_{i=1}^{2} (F_B)_i$$
$$V = Ri + L\frac{di}{dt} + K_{vB}\frac{dx_v}{dt} \tag{1}$$

where, K_m & K_v : DDV motor force constant and spring rate of DDV spool

M_v & B_v : Mass and damping coefficient of DDV spool

R & L : Resistance and inductance of DDV coil

K_{vB} : Back EMF constant of DDV motor

$(F_B)_i$: Flow induced force for hydraulic system #i.

The following Eq. (2) is obtained by applying the continuity equation of fluid flow on DDV actuator chambers and combining the load flow equation (Merritt, 1967).

$$Q_L = K_q x_v \sqrt{P_s - sign(x_v) P_L} \approx K_q x_v - K_c P_L$$

$$=A\frac{dY_{P/B}}{dt}+\frac{V_t}{4\beta}\frac{dP_L}{dt}+(C_{ip}+C_{ep}/2)P_L \quad (2)$$

where, K_q & K_c : flow gain and flow-pressure coefficient

A & V_t : DDV actuator piston area and total chamber volume

β : Bulk modulus of operating oil

C_{ip} & C_{ep} : Internal and external leakage coefficient.

$Y_{P/B}$ in Eq. (2) means the relative displacement of piston to actuator body, and is the same one picked up by the LVDT sensor installed on the body.

$$Y_{P/B}=Y_P-Y_B=Y_P-(-2P_LA)/K_B$$
$$=Y_P+2P_LA/K_B \quad (3)$$

By the substitution of Eq. (3) into (2), the following Eq. (4) is made.

$$Q_L\approx K_qx_v-K_cP_L=A\frac{dY_P}{dt}+(\frac{V_t}{4\beta}+\frac{2A^2}{K_B})\frac{dP_L}{dt}$$
$$+(C_{ip}+C_{ep}/2)P_L \quad (4)$$

The last equation governing the DDV actuator dynamics is the Newton's equation, in which the inertial effect of control surface and hinge moment are considered.

$$2AP_L-\frac{M_h}{R}=M_L\frac{d^2Y_P}{dt^2}+B_L\frac{dY_P}{dt}+K_LY_P \quad (5)$$

where, M_L : Equivalent mass of control surface inertia

B_L : Damping coefficient of control surface

K_L : Spring constant

M_h & R : Hinge moment and actuator horn radius.

By combining DDV dynamics, and Eq. (4) and (5), the block diagram of Fig. 2 is concluded. For a simpler presentation, the DDV spool dynamics of Eq. (1) and servo drive amplifier characteristics are contained inside the box in this figure. The filter dynamics and feedback gains in Fig. 2 are determined to meet the DDV actuator outer loop frequency response requirement (Hsu, 1991).

The lower part of Fig. 2 describes the dynamics of load replicating actuator, which are governed by the following equations of (6) and (7), and

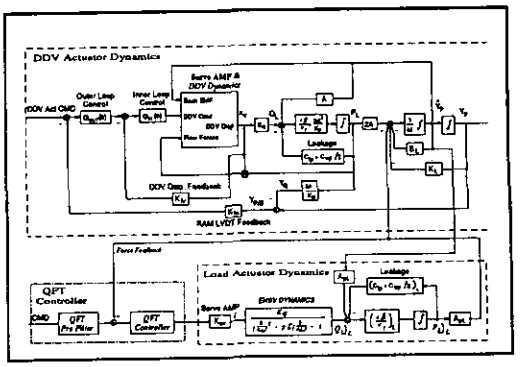

Fig. 2 Linear model of DLS dynamics with QFT control (Model #1)

the structure of QFT force control loop.

$$Q_L^*=A_{pL}\frac{dY_L}{dt}+\frac{V_t^*}{4\beta}\frac{dP_L^*}{dt}$$
$$+(C_{ip}^*+C_{ep}^*/2)P_L^* \quad (6)$$

where, $\bullet^*$: parameters for load actuation system

A_{pL} : load actuator piston area

$Y_L(=Y_P)$: load actuator displacement.

Based on the manufacturer's catalog for MOOG D761 series servo valve (MOOG, 1997), the load flow equation can be modeled as follows:

$$\frac{Q_L^*(s)}{i(s)}=\frac{K_{qi}}{(s/\omega_n)^2+2\zeta(s/\omega_n)+1} \quad (7)$$

where, K_{qi} : flow gain of servo valve $(in^3/s/mA)\in[1.8187, 3.6374]$

ω_n : natural frequency of servo valve (Hz)$\in[30, 65]$

ζ : damping ratio of servo valve$\in[1.1, 1.7]$.

2.2 Model #2 for DLS dynamics

The modeling of DDV actuator can be simplified a lot more than that of the above. In considering the force fight between DDV and load actuator in the normal operation of DLS, the DDV actuator can be modeled as a simple spring having the equivalent stiffness K_{EFF} of as described in Fig. 3.

$$K_{EFF}=(\frac{1}{K_B}+\frac{1}{K_{ACT1}+K_{ACT2}}+\frac{1}{K_{RD}})^{-1} \quad (8)$$

In the above Eq. (8), K_{ACT1} and K_{ACT2} re-

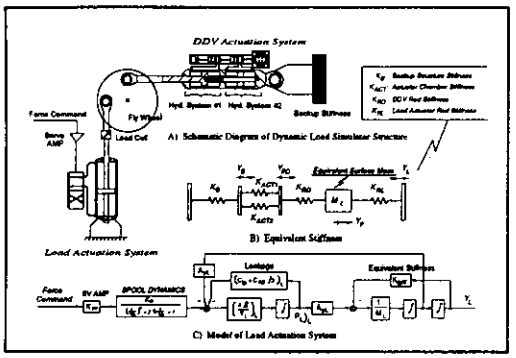

Fig. 3 DLS stiffness and model of load actuator (Model #2)

present the DDV actuator stiffness for the hydraulic system #1 and #2, respectively, which are caused by the trapped oil inside two oil chambers. All the inertial effect of DLS can be applied to the load actuator dynamics as follows.

$$M_L\frac{d^2Y_L}{dt^2}=A_{pL}P_L+K_{EFF}Y_L \tag{9}$$

By combining the above equations with the flow continuity equation of (6) and load flow equation of (7), the model #2 structure of DLS of Fig. 3(C) can be defined.

2.3 Comparison of model #1 and #2 with experimental results

The accuracy of modeling is verified through the comparison with experimental results. The load actuation system interconnected with the fully pressurized DDV actuator as 3,000 psi is excited by 1 kHz band-limited Pseudo Random Binary Sequence (PRBS) of 2.0 V_{pp}, and 3.8 V_{pp}, and the developed force on the piston rod is picked up by the load cell (SENSOTEC Model 41). Figure 4 shows the experimental frequency response with the analytic ones, which are plotted as dot line for the model #1 and dashed lines for the model #2. The analytical frequency response for the model # 1 is calculated for the nominal condition of mid values of K_{qi}, ω_n, & ζ in nonlinear servo valve dynamics as described in Eq. (7), and those for the model #2 are from two extreme conditions in Eq. (7). The Bode plot showing the higher gains at low frequency region

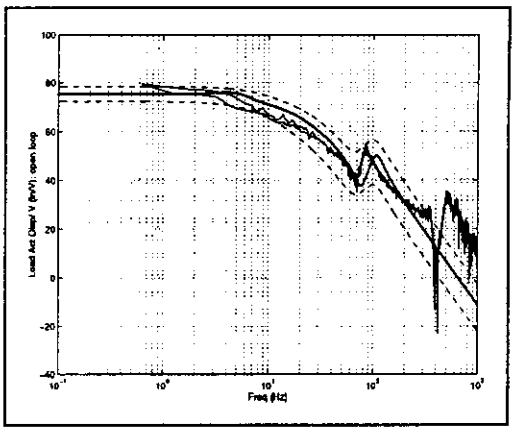

Fig. 4 Comparison of analytic and experimental open loop frequency response

corresponds to the experimental frequency response obtained by the high power input. Any theoretical model is not proper in predicting the experimental results due to discrepancies in gains at low frequency and resonant peak frequency about 85 Hz. The large variations of DC characteristics in experimental frequency responses are considered as the effect of equivalent stiffness change of DLS by input signal magnitude. Because of bearings, and mechanical couplings in DLS, the stiffness of DLS will be minimal at the low input power excitation. As clearly shown in Fig. 4, any one analytical LTI model can not represent the whole nonlinear dynamics of DLS. Therefore, a robust feedback controller is to be designed for these uncertain plant dynamics to achieve a uniform performance and stability requirements, which is the main theme of the following section.

3. Force Control System Design Using QFT

QFT is a one method of designing robust control system (Reynolds, 1996, Snell, 1996, and D'Azzo, 1988). For an uncertain servo valve dynamics described in Eq. (7), two degree of freedom force controllers which have the structure shown in Fig. 2 are designed to meet the following specification of load replication system.

3.1 Design specification on QFT force controller

The QFT force control loop of the load actuation system is to be designed to meet the following upper and lower tracking boundary specifications of

$$T_L(s)=\frac{0.98}{(s/308+1)(s/308+1)(s/880+1)}$$
$$T_U(s)=\frac{1.02}{(s^2/242^2+2\times0.8s/242+1)(s/990+1)(s/6594+1)} \quad (9)$$

These boundaries are determined from the requirements of 30 Hz bandwidth, peak overshoot less than 10%, and steady state error less than 2% for the closed loop load actuation system. Except these requirements, the stability margins of 5 dB gain and 45° phase are assumed, which are automatically satisfied when all the perturbed loop gain Bode plots due to uncertainties exist outside of 2 dB M-circle shown in Fig. 5.

3.2 QFT force controller design

The templates at the frequency of $\omega_T(r/s)\in$ [10, 16.7, 27.8, 46.4, 77.4, 166.8, 359.4, 599.5, 1291.5, 2154.4, 2782.6, 3593.8, 4641.6] are also shown in this figure as the dotted boundaries, which are caused by the nonlinear characteristic of servo valve flow dynamics of Eq. (7). The relatively larger templates are observed at the servo valve natural frequency range (188.5—408.4 r/s), and templates for low and high frequency are determined mainly from the magnitude variation of servo valve flow gain. The points designated by '*' at each frequency of ω_T in this figure means the Nichols plot of the nominal plant, that is defined for the condition of minimum flow gain, natural frequency, and damping in Eq. (7).

The QFT force controller that guarantees the closed loop load actuation system to meet the performance and stability requirements for the given plant uncertainties of Eq. (7) can be found by placing the Nichols plot of nominal plant loop gain function over the tracking bounds for each specific frequency. As shown in Fig. 5, the Nichols plot data of the nominal plant for the frequency of $\omega_B(r/s)\in$[10, 16.7, 27.8, 46.4, 77.4, 359.4, 599.5, 1291.5] are located above the matching tracking bounds by selecting the QFT controller as

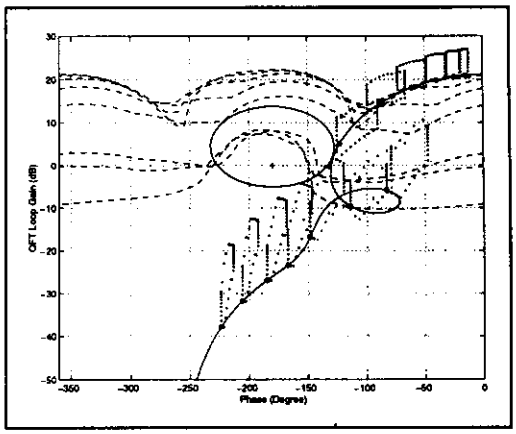

Fig. 5 Nichols plot of QFT design

$$G(s)=\frac{0.002704(s/501+1)(s/823+1)}{(s^2/3107^2+2\times0.6s/3107+1)} \quad (10)$$

Slight invasion of template to the 2 dB M-circle at the frequency of 200-300 r/s can be seen in Fig. 5, which means imperfect fulfillment of stability margin requirement. However, this can be accepted as the satisfactory design, considering that there is no significant impact on phase, or gain margin.

Loop shaping by $G(s)$ of Eq. (10) guarantees only that the magnitude variations in closed loop Bode plot due to plant uncertainties are within the range of $|\delta(j\omega)|=|T_U(j\omega)-T_L(j\omega)|$ at each frequency. Therefore, a pre-filter like the one of Eq. (11) is required to make the closed loop $T(j\omega)$ lie between the frequency domain performance specifications of Eq. (9).

$$F(s)=\frac{1.065(s/160+1)}{(s/108+1)(s^2/756^2+2\times0.7s/756+1)} \quad (11)$$

4. Evaluation of QFT Force Control System Design

The frequency response of the QFT closed loop load actuation system is compared with the upper ($T_U(j\omega)$) and lower ($T_L(j\omega)$) performance bounds in Fig. 6. The Bode plots shown as the

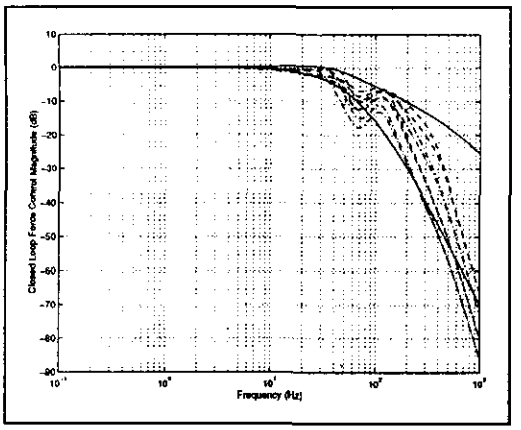

Fig. 6 Closed loop frequency response of QFT design

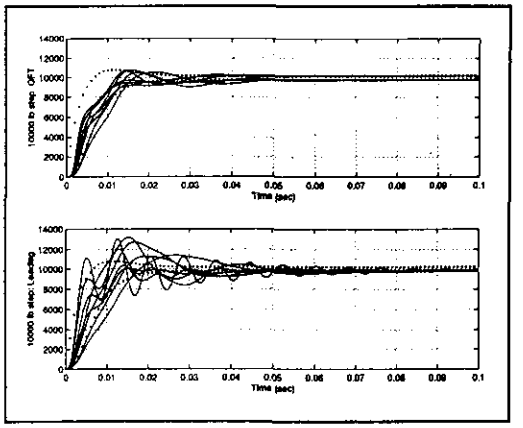

Fig. 7 Time domain step responses (QFT & Lead-Lag) design

dashed lines in this figure are for 8 extreme case dynamics from the uncertain servo valve characteristics, which are obtained from the mini-max value combination of K_{qi}, ω_n, & ζ in Eq. (7). All the extreme case dynamics are almost within the desired performance specification except the frequency region ranging from 34 Hz to 90 Hz and the high frequency region above 230 Hz. The effect of poor achievement on performance bounds requirement at the mid-frequency range of 50 Hz is well noticed in Fig. 7 which shows the step response comparison between QFT and the following lead-lag controller design of Eq. (12).

$$K(s)=\frac{0.0091(s/48.4+1)(s/115.5+1)}{(s/4.05+1)(s/346+1)} \quad (12)$$

The almost identical design requirements are applied for the lead-lag control system design, in which the nominal plant dynamics having the mid values of K_{qi}, ω_n, & ζ in Eq. (7) is assumed. The dotted lines in these figures denote the step responses obtained from the two performance bounds of Eq. (9), and solid lines are from 8 extreme cases with QFT and lead-lag controller respectively. From these time domain responses, the superiority of QFT over lead-lag design is well understood. In case of lead-lag control, a large overshoot and settling time are noticed for plant dynamics variation specified by Eq. (7), even though the lead-lag force control system design is satisfactorily made for the above mentioned nominal plant condition. However, the step responses for QFT design also show some poor performance in transient response region, which results from imperfect achievement in the closed loop frequency requirement of Fig. 6 at the mid-frequency range of 50 Hz. On the other hand, the deviation from the performance bounds at the high frequency region above 230 Hz is a rather favorable characteristic in terms of un-modeled high frequency dynamic and sensor noise effects.

The problems of slight penetration of 2 dB M-circle in Fig. 5 and breakaway from tracking boundary requirement in Fig. 6 can be resolved by using more complicated and high bandwidth QFT compensator. However, this design demands more computational delay and high sampling rate in the controller implementation. Therefore, the experimental verification is to be made with the current design.

5. Conclusion

An aircraft actuation system test rig, dynamic load simulator, which can reproduce, on-ground, the aerodynamic hinge moment of control surface, is introduced. Two mathematical models for dynamic load simulator are developed, and tested for their validity with the experimental results. Especially, the nonlinear dynamic characteristics of electro-hydraulic servo valve of load replication system are represented with a linear system

using the parametric uncertainties in valve flow gain, natural frequency, and damping. A nominal model for DLS dynamics, and suitable uncertainty bounds are proposed by the comparison of this analytic model with the experimental results. A QFT force control system is designed for dynamic load simulator to uniformly replicate on-ground aerodynamic hinge moment even for the uncertain dynamic characteristics of load actuation system servo valve. The efficacy of QFT force control system is verified by numerical simulation, in which hydraulic actuation system dynamics of aircraft control surface is considered.

References

Boeing Commercial Airplane Company, 1985, "Test Act System Validation Final Report," *NASA CR-172525*.

D'Azzo, J. D' and Houpis, C. H., 1988, *Linear Control System Analysis and Design Conventional and Modern*, McGraw-Hill.

Hsu, Y. N., Lai, C. Y., Hsu, M. H. and Lee, Y. K., 1991, "Development of the Direct Drive Valve (DDV) Actuation System on the IDF Aircraft," *International Pacific Air and Space Technology Conference*.

Merritt, H. 1967, "Hydraulic Control Systems," *John Wiley & Sons*.

MOOG, 1997, *Servo and Proportional System Catalog*, pp. 95~98.

Nam, Y., Lee, J. and Hong, S. K., 2000, "Force Control System Design for Aerodynamic Load Simulator," *Proceedings of the American Control Conference*, pp. 3043~3047.

Reynolds, O. R., Pachter, M. and Houpis, C. H., 1996, "Full Envelope Flight Control System Design Using Quantitative Feedback Theory," *Journal of Guidance, Control, and Dynamics*, Vol. 19, No. 1, pp. 23~29.

Roskam, J., 1979, "Airplane Flight Dynamics and Automatic Flight Controls," Roskam Aviation and Engineering Corporation.

Schaefer, W. S., Inderhees, L. J. and Moynes, J. F., "Flight Control Actuation System for B-2 Advanced Technology Bomber," *Technical Bulletin 153, MOOG*.

Snell, S. A. and Stout, P. W., 1996, "Quantitative Feedback Theory with a Scheduled Gain for Full Envelope Longitudinal Control," *Journal of Guidance, Control, and Dynamics*, Vol. 19, No. 5, pp. 1095~1101.

Vieten, K. W., Snyder, J. D. and Clark, R. P., 1993, "Redundancy Management Concepts for Advanced Actuation Systems," *AIAA/AHS/ASEE Aerospace Design Conference*, AIAA 93-1168, pp. 1~9, Feb.